

PRUDENCE Deliverable 5.A.6

## **Precipitation extremes over the Mediterranean**

by

**Tom Holt and Jean Palutikof**

**Climatic Research Unit,  
University of East Anglia,  
Norwich, UK**

**February, 2004**



# 1 Introduction

This deliverable assesses predicted changes in Mediterranean precipitation extremes from four regional climate models (RCMs). Annual indices of precipitation extremes are calculated for the periods 1960-1990 and 2070-2100. Following a comparison of the differences between mean extremes for the two periods, the analysis continues by comparing return levels calculated using the properties of the Generalised Extreme Value (GEV) distribution.

## 2 The models

The HadRM3P and SMHI models are chosen because they offer the common period 1960-1990, together with A2a and B2a scenarios for the future (2070-2100). A2 and B2 refer to the IPCC SRES emissions scenarios, with A2 being the more severe. Lowercase 'a', 'b', and 'c' are used to distinguish between different ensemble members. At the time of writing, PRUDENCE models only offer one ensemble member, with the exception of HadRM3P which offers three. The SMHI regional model provides two variants: one with boundary conditions taken from a Hadley Centre (HC) global climate model, and the other using Max Planck Institute (MPI) forcing. The final model used in this study is the Danish Meteorological Institute (DMI) model using HC forcing but only providing the A2a scenario for future precipitation.

## 3 The indices of extremes

Using daily data from each model, the following annual indices of precipitation extremes are calculated:

1. Total number of days in a year with rainfall higher than 10 mm (nGT10)
2. Total number of days in a year with rainfall higher than 20 mm (nGT20)
3. Maximum length of dry spell in a year (in days) (MaxDrySpell)
4. Maximum length of wet spell in a year (in days) (MaxWetSpell)
5. Start of MaxDrySpell (day in the year) (StartDrought)
6. End of MaxDrySpell (day in the year) (EndDrought)
7. Annual maximum running total rainfall over three days (MaxRunSum3)

Although the start and end of maximum dry spell are not really extremes, the timing of the long dry Mediterranean summer period is of great interest to the agriculture and tourism industries. Any permanent shifts in start and end dates have important implications for planning such things as accommodation, leisure facilities, fire services, transport, and planting and harvesting.

## 4 Analysis – difference maps

The models used in this study contain error associated with imperfect knowledge of physical processes and limitations in computing resources. Since each model is formulated differently, the error will cause differences in the results. Assuming that the models are of similar quality, however, it is reasonable to assume that predictions of future climate under the same forcing scenario will be broadly similar. It is also reasonable, therefore, to present an average of the results of all models and expect the average predicted climate to be a more statistically robust representation of future conditions than the results from any single model. One danger with this approach is that two models may have results with opposite sign over large areas, giving a very smooth averaged field. To show that this is not the case, we present the results from each model in an Appendix so that the broad similarities between them can be readily assessed. The Appendix contains seven difference maps (four A2a model runs and three B2a model runs) for each of the indices described above. Here, we present four maps for each index:

1. A map of differences for each index was created by subtracting the mean 1960-1990 index from the mean 2070-2100 index. The annual indices for each model were first interpolated onto a common  $0.5^\circ \times 0.5^\circ$  grid. Then the mean over the 30 years was calculated for each model and the difference, 2070-2100 minus 1960-1990, calculated. Finally, the average difference across all seven model runs was calculated. The average difference over the four models of the A2a scenario is presented in the first map for each index. For example, Figure 1a shows the mean difference between the nGT10 index for the A2a scenario and the common period over all models. Since the common period is subtracted from the future, negative values indicate less rain in the future, positive values – more rain.
2. It is important to know how confident we can be in the estimated future changes in rainfall. The second figure, therefore, shows the 95% confidence range calculated by bootstrapping the differences between indices in the two periods. The bootstrapping procedure resamples the differences 1000 times with replacement, calculating the mean difference on each iteration. The resampling is from a sample of 124 for the A2a scenario (four models with 31 annual extremes each), and a sample of 93 for the B2a scenario (three models with 31 annual extremes each). An alternative, and arguably more robust, methodology would be to resample the indices over all models for each period 1000 times, calculating the differences between the resampled series each time. This method removes the pairing between the series and makes greater use of available variance in the data. In fact, confidence limits derived from both methods are virtually identical, with the differences being no greater than one might expect by simply repeating the resampling using either method. Since resampling the differences takes less than half the time to run, this is our preferred technique for generating confidence intervals.

The method of choosing confidence limits is Effron's percentile method, bias adjusted (Davison & Hinkley, 1997). It would be cumbersome to show maps of the upper and lower confidence limits, so we show the difference between them, termed the confidence range. The upper and lower bounds can be approximated by dividing the range by two and adding or subtracting that value from the mean difference. For example, over the Alps in Figure 1b the confidence range is about 8 days. The mean from Figure 1a is about -10 days, indicating that in future the number of days in a year with rainfall higher than 10 mm can be expected to be about 10 days less than at present. Using the additional information from Figure 1b, we can say that we are 95% confident that the reduction in the number of days with rainfall above 10 mm over the Alps will be between 6 ( $-10 + 4$ ) and 14 ( $-10 - 4$ ) days. In other words, there is a large amount of uncertainty in the estimate of changes in rainfall over the Alps, amounting to  $\pm 40\%$  of the prediction. Note that, although the confidence limits tend to increase with the magnitude of the predicted mean, this is not always the case. For example, over the eastern Adriatic coast, the drying is predicted to be higher than over the Alps (Figure 1a), yet the confidence range is almost halved (Figure 1b). In this case, the uncertainty in the prediction is about  $\pm 18\%$  (derived from a prediction of about -14 days and confidence limits of  $\pm 2.5$  days).

3. The third map in each group of four presents the pattern of mean difference under the B2a scenario.
4. The fourth map shows the 95% confidence range for the B2a predictions.

## 4.1 nGT10 differences

Figures 1a to 1d show the difference between the means together with the 95% confidence range for the number of days in a year with rainfall higher than 10 mm (nGT10) for the A2a and B2a scenarios. Under the A2a scenario, Figure 1a indicates that we can expect future reductions in nGT10 over northern Portugal and Spain, the Alps, central and southern Italy, and the eastern Adriatic coast. The range of uncertainty about these predictions ranges from  $\pm 40\%$  over the Alps to  $\pm 18\%$  over the eastern Adriatic (Figure 1b). With the B2a scenario, the future drying is reduced (Figure 1c). Uncertainty is also reduced under the B2a scenario in all areas apart from those with greatest drying, such as the Alps (Figure 1d).

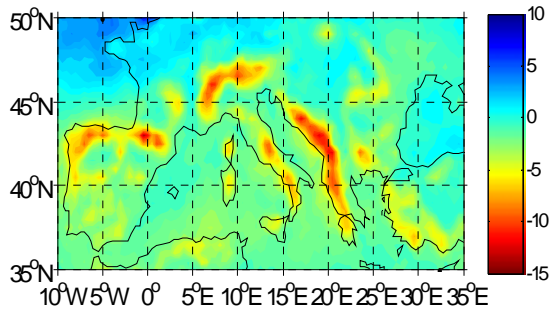


Figure 1a A2a - nGT10

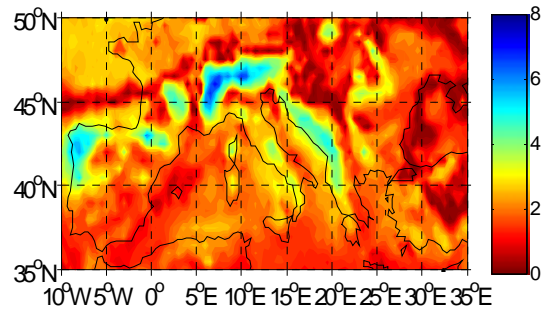


Figure 1b A2a confidence range (days)

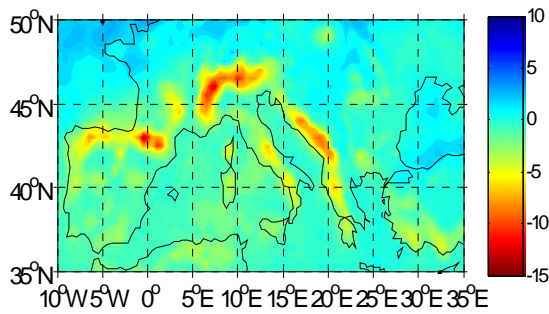


Figure 1c B2a - nGT10

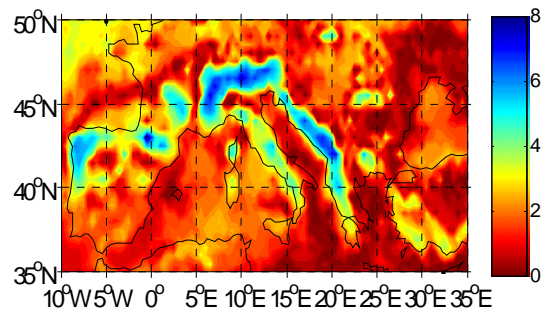
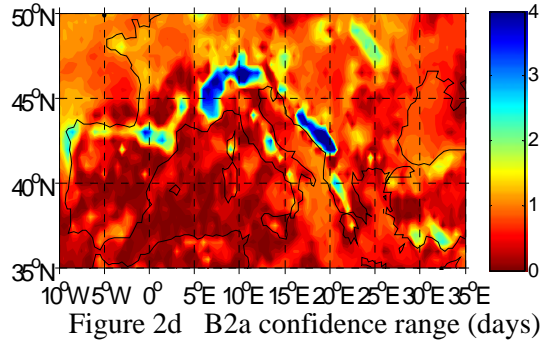
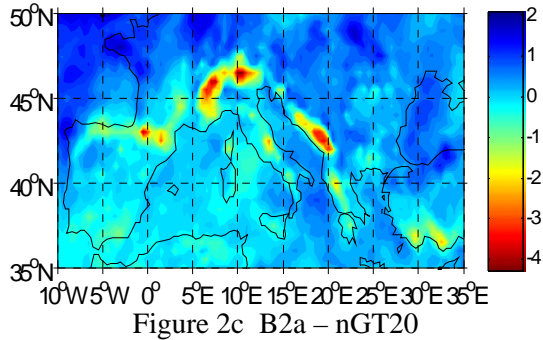
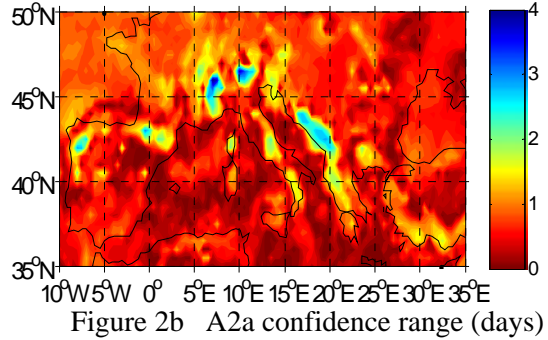
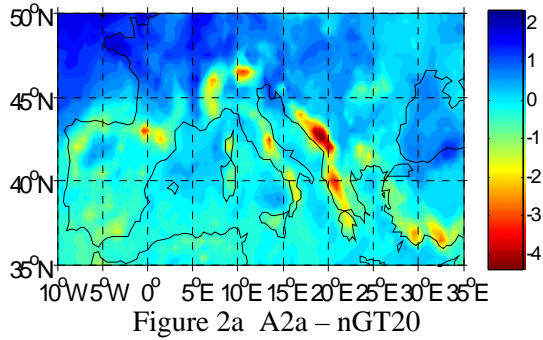


Figure 1d B2a confidence range (days)

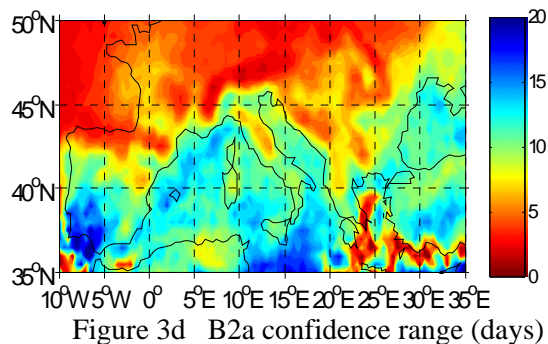
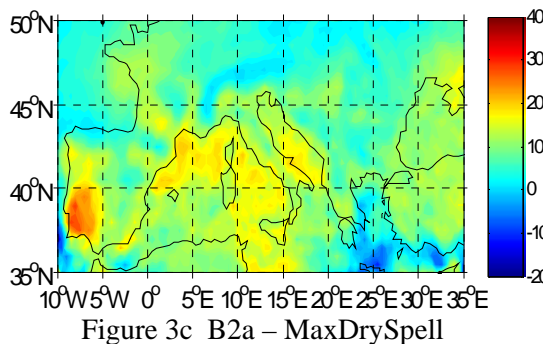
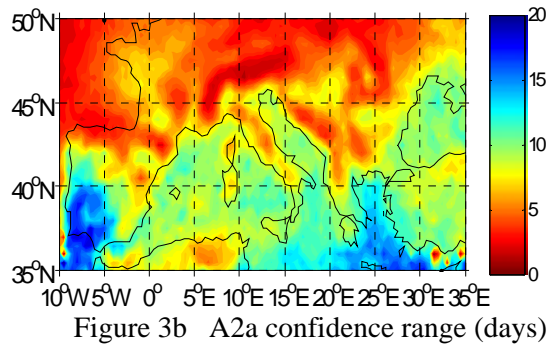
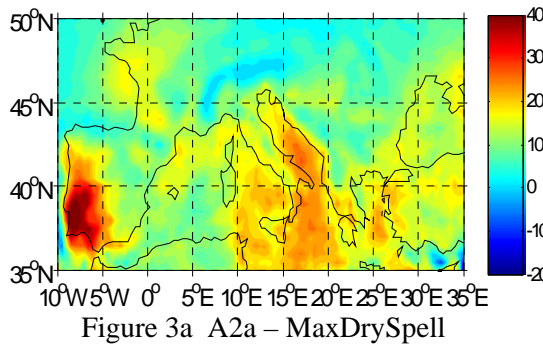
## 4.2 nGT20 differences

The results for the number of days with rainfall higher than 20 mm (nGT20) in Figures 2a to 2d are similar to those for nGT10, but with changes of much shorter duration. An important difference is that the high intensity rainfall events are predicted to become much less frequent over the Alps under the B2a scenario (Figure 2c) than under the A2a scenario (Figure 2a). However, the uncertainty in this particular prediction is very high at  $\pm 50\%$  (Figure 2d).



### 4.3 MaxDrySpell differences

All the duration indices used in this study are based on a definition of a day with rainfall having at least 0.5 mm of rain. This threshold was determined by trial and error as giving the closest agreement with station data. The length of the maximum dry spell in a year (that is, the summer drought period in the Mediterranean region) is predicted to extend by up to 40 days in southern Portugal (Figure 3a) and by up to 20 days in southern Italy and Greece. The uncertainty in these predictions is  $\pm 7$  days and  $\pm 4$  days, respectively. The B2a scenario (Figure 3c) indicates that the drying would be halved with reduced emissions but Figure 3d suggests that there is more uncertainty about the B2a prediction than about the A2a prediction (Figure 3b).



#### 4.4 StartDrought differences

Changes in the start of the maximum length of dry spell are important for both the tourist and agriculture industries in the Mediterranean. In Figures 4a to 4d, the scale is Julian Day number, and the colouring convention assumes that a predicted future earlier start of the dry spell is likely to be associated with a longer dry spell, that is, more red. It is important to note that this is just a convention, Figures 4a to 4d say nothing about the length of the dry spell.

The A2a scenario is associated with a future earlier start to the longest dry spell over nearly all the Mediterranean (Figure 4a). Interestingly, this map also indicates that eastern France, Switzerland, and southern Germany can expect a markedly later start to the longest dry spell. However, Figure 4b shows that the uncertainty about this predicted later start is of the order of  $\pm 50\%$ . For the Mediterranean, the drought is predicted to start 15 to 20 days earlier (Figure 4a) with uncertainty  $\pm 3$  to  $\pm 6$  days. The biggest change is forecast for North Africa, but this also has very high uncertainty (about  $\pm 60\%$ ). The B2a scenario (Figure 4c) shows weaker changes in the start date of drought, but following the same general pattern as the A2a scenario (Figure 4a).

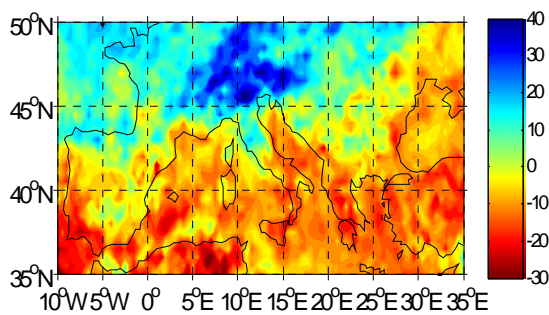


Figure 4a A2a – StartDrought

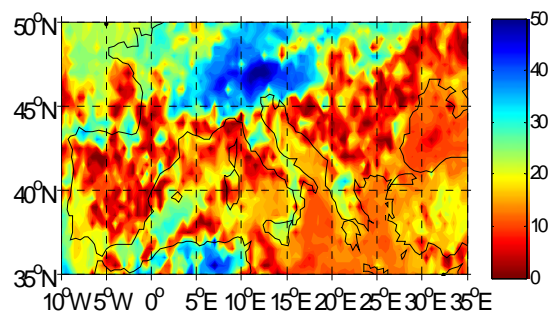


Figure 4b A2a confidence range (days)

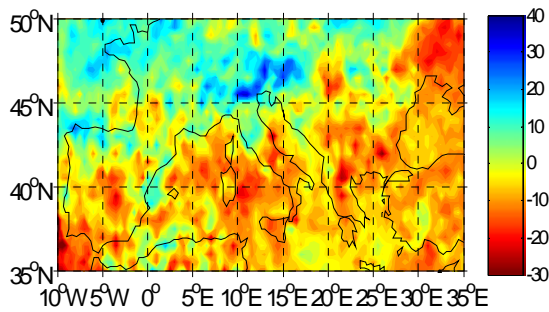


Figure 4c B2a – StartDrought

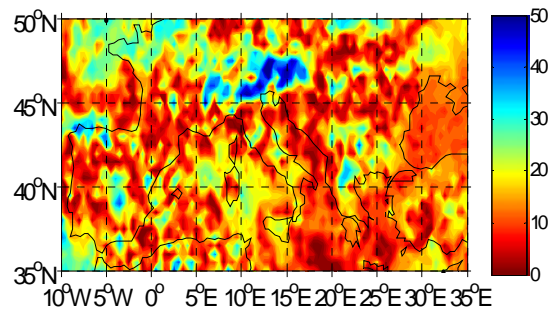
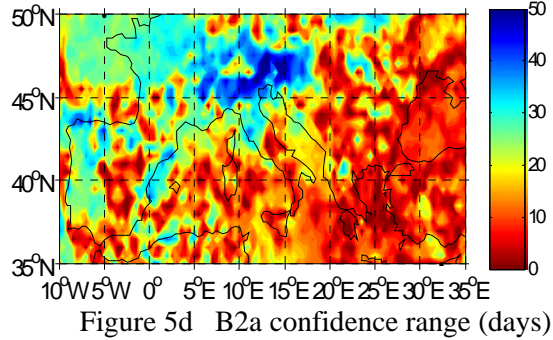
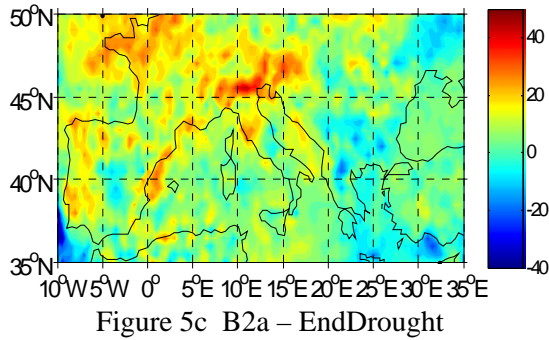
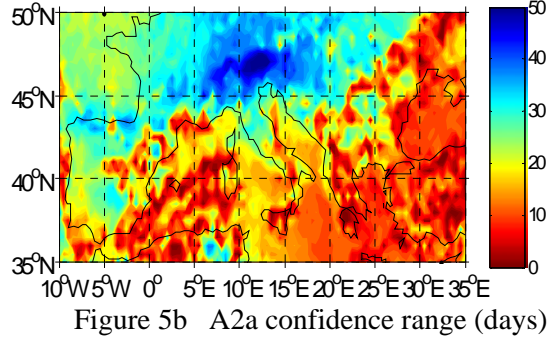
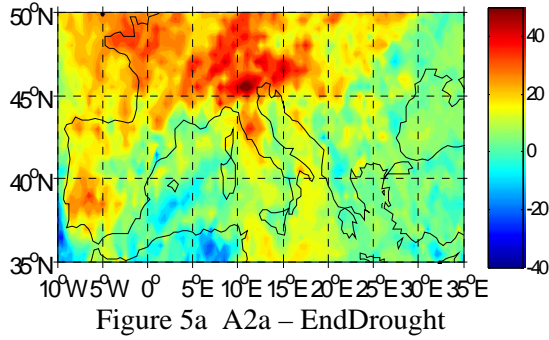


Figure 4d B2a confidence range (days)

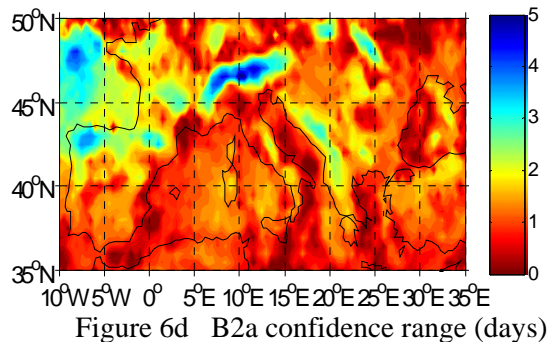
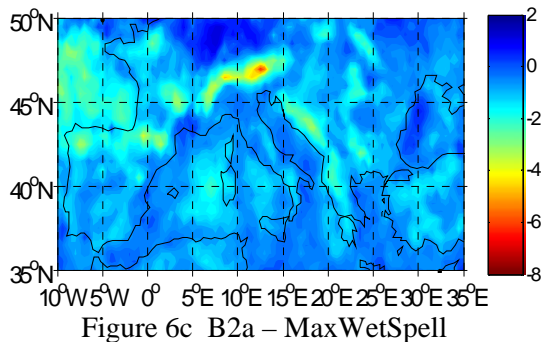
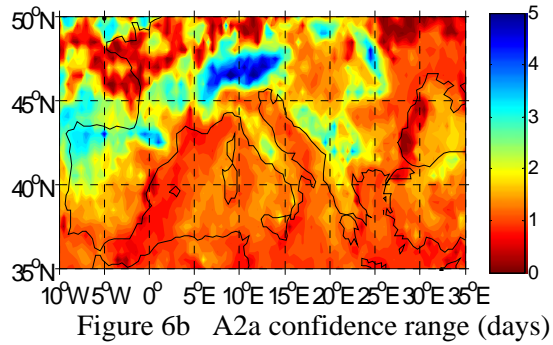
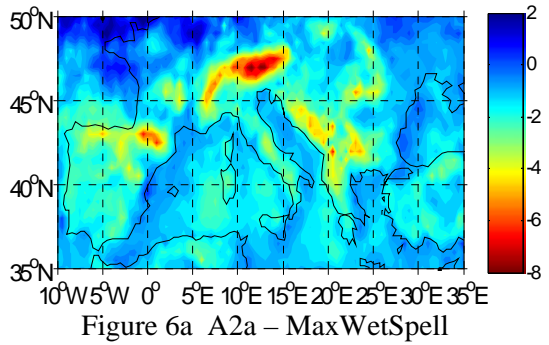
#### 4.5 EndDrought differences

The predicted future changes in timing of the end of drought (Figures 5a to 5d) follow the opposite colouring convention of the start of drought (Figures 4a to 4d). That is, increasing red is associated with later end of drought and an assumed extension of drought. In fact, Figure 5a indicates that the region associated with later start to drought in Figure 4a is also associated with later end of drought. Thus, the maximum dry spell length over eastern France, Switzerland, and southern Germany is predicted not to change (as can be confirmed by examining Figure 3a) but to occur later in the year. Again, there is quite high uncertainty (about  $\pm 50\%$ ) about changes in the end of drought over these areas (Figure 5b). Since Figure 5a also shows that the end of drought will change little over most of the Mediterranean, and we know from Figures 3a and 4a that drought will be longer over this region, we can say that drought will be prolonged by starting earlier. The B2a scenario (Figures 5c and 5d) shows considerable reduction in the effects of the A2a scenario.



#### 4.6 MaxWetSpell differences

The predicted changes in the length of the annual maximum wet spell (Figure 6a) reveal that it will be shorter under the A2a scenario over northern Spain, the Alps, and the eastern coast of the Adriatic. The uncertainty in the prediction over the Alps is about  $\pm 50\%$  (Figure 6b) but less pronounced in the other areas. Figures 6c and 6d show that the predicted changes are much reduced under the B2a scenario.



## 4.7 MaxRunSum3 differences

The annual maximum running total rainfall over three days is expected to fall over most of the southern Mediterranean, particularly southern Spain and Portugal, and increase over parts of the northern Mediterranean under the A2a scenario (Figure 7a). Under the B2a scenario (Figure 7c), rainfall will increase over southern Italy, the Alps, and northern Portugal. The greatest uncertainty (about  $\pm 60\%$ ) is associated with the prediction over the Alps under the B2a scenario (Figure 7d).

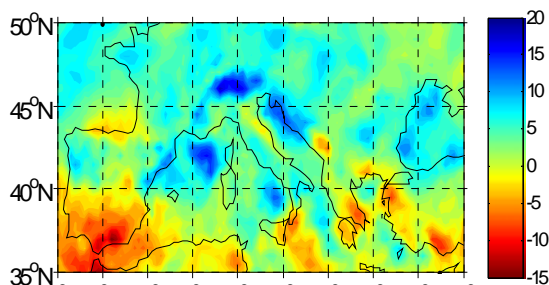


Figure 7a A2a – MaxWetSpell

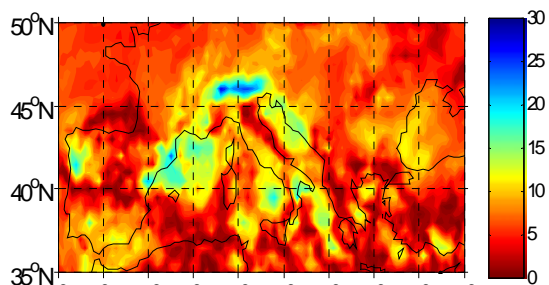


Figure 7b A2a confidence range (days)

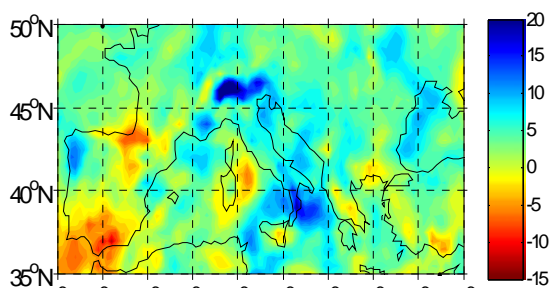


Figure 7c B2a – MaxWetSpell

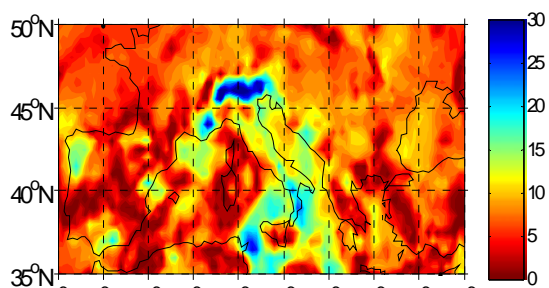


Figure 7d B2a confidence range (days)

## 4.8 Summary of difference pattern analysis

The Appendix contains detailed comparisons between extremes from all the models used in this study. The predicted changes in future precipitation are sufficiently consistent to justify averaging their results to give a mean prediction. Uncertainty in the mean prediction is estimated by bootstrapping the changes over all model years for each scenario. One of the most important findings is that changes in precipitation due to differences in forcing are about the same magnitude as the difference in changes predicted under the A2a and B2a scenarios.

Predicted changes in precipitation indices between the periods 1960-1990 and 2070-2100, under the A2a emissions scenario, indicate considerable drying over much of the Mediterranean. The main features are reduced intensity rainfall, earlier start of drought, and longer drought. The regions most affected are the southern Iberian peninsula, the Alps, the eastern Adriatic seaboard, and southern Greece. Although the B2a scenario provides considerable mitigation, being associated with increased rainfall in some areas, the overall pattern is still one of a drier Mediterranean.

## 5 Analysis – return levels

It is possible to estimate the probability of a climate variable reaching a particular magnitude in terms of a return period. For example, we could say that, on average, we expect daily total rainfall at a given location to exceed 30 mm once every 20 years. From this example, the 20 years frequency is known as the return period (or interarrival time), and the amount of rain – 30 mm/day, is known as the return level for that return period. If the statistical distribution of the data is known, we can use this to estimate return levels over any return period, including periods beyond the range of the observations. There is a limit to the amount of extrapolation that is practical, or advisable, because the statistical properties of climate vary with time. For example, it would be pointless to estimate 10000 year return levels from 100 years of data! However, return periods of about three times the length of the observed series are feasible.

Here, we compare the return levels at 50 and 100 years for the indices of extremes described in the previous section. The statistical model we fit is the Generalised Extreme Value (GEV) distribution (Coles, 2001), which applies to maxima over a block interval – generally a year. Only three of the indices of extremes fulfill this criterion. These are:

1. Annual maximum running total rainfall over three days (MaxRunSum3)
2. Maximum length of dry spell in a year (in days) (MaxDrySpell)
3. Maximum length of wet spell in a year (in days) (MaxWetSpell)

The procedure is as follows:

1. Calculate the GEV location, scale, and shape parameters for each index at each grid square
2. Use these to estimate the mean and variance of the fitted GEV model at each grid square. This is not the same as the mean and variance in standard use (based on assumed normally distributed data), but is adjusted for the “heavier” tails of extreme value distributions using the gamma function.
3. Use the GEV mean, variance, and shape parameters to estimate return levels (Coles, 2001)

It is important to understand that model extremes will not always fit the GEV model perfectly. In fact, for some grid squares it is impossible to estimate return levels. This is because valid values of the GEV variance and mean are constrained by the shape parameter. Here, if the properties of the data are such that either the mean or variance do not exist, the return level is assigned missing value status.

### 5.1 MaxRunSum3

To continue the explanation of return level analysis, the results for an analysis of MaxRunSum3 from HadRM3P are described in detail here. The results for other models, and for maximum dry spell and maximum wet spell, are presented in summary form only.

Figures 8a to 8c map the HadRM3P return levels for a 50 year return period for the common period (1960-1990), and for the A2a, and B2a scenarios, respectively. The results for a 100 year return period are shown in Figures 9a to 9c. Because the maps are dominated by a small area of very high rainfall over the Swiss Alps, the scaling has been adjusted to provide more information at lower amounts of rainfall. The maximum rainfall under the future scenarios is actually 800 mm for the 50 year return period and 900 mm for the 100 year return period. These are highly suspect amounts of rainfall but they are very limited in extent. The very dark red areas, particularly evident for the A2a and B2a scenario plots, indicate areas where the GEV model failed to provide either a valid mean or a valid variance.

50 year return period

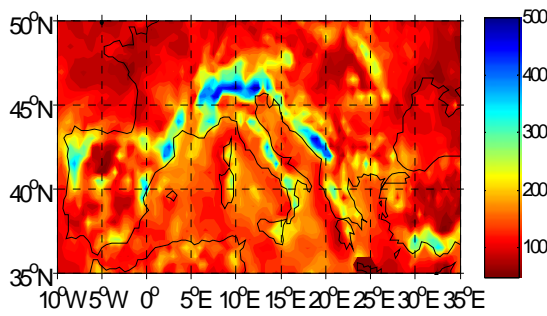


Figure 8a Hadrm3Pcom MaxRunSum3 (mm)

100 year return period

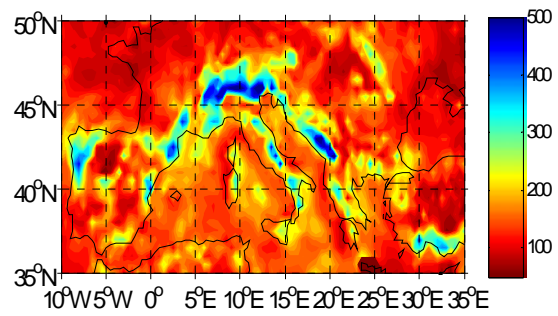


Figure 9a Hadrm3Pcom MaxRunSum3 (mm)

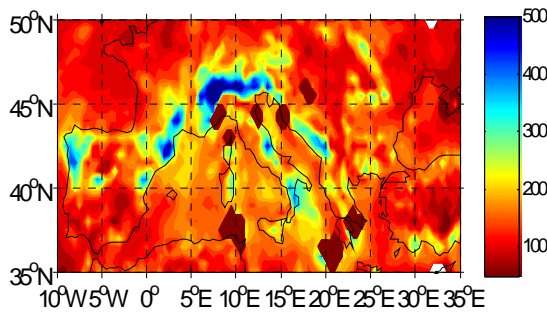


Figure 8b Hadrm3PA2a MaxRunSum3 (mm)

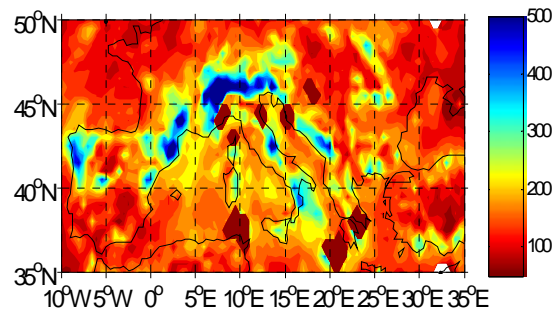


Figure 9b Hadrm3PA2a MaxRunSum3 (mm)

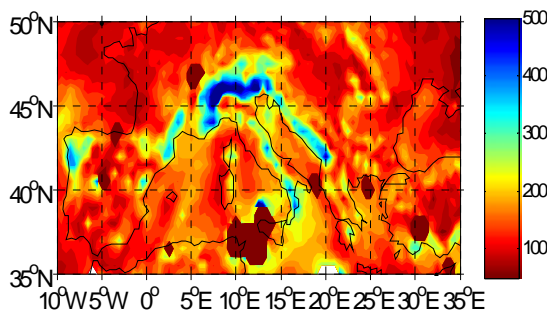


Figure 8c Hadrm3PB2a MaxRunSum3 (mm)

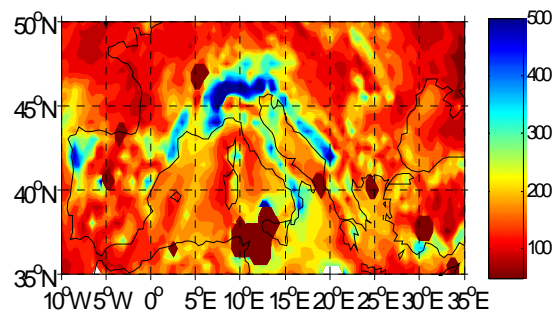


Figure 9c Hadrm3PB2a MaxRunSum3 (mm)

The figures show that the 100 year return levels have the same pattern as the 50 year levels but are about 50 mm higher. However, it is not easy to determine the nature of changes between the common period and the A2a and B2a scenario. We can summarise the differences by subtracting the common period return level pattern from that of the A2a and B2a scenarios. The differences for 100 year return levels are shown in the next set of diagrams for all models.

With the exception of the SMHI model using Hadley Centre Forcing (Figures 11a and 11b), all models exhibit isolated pockets of very high return levels, as described above for HadRM3P over the Swiss Alps. The effect of these has been diminished by scaling the contour shading to reasonable bounds appropriate for all models. The easiest way to interpret Figures 10a to 13a is to note that colours from light green, through yellow, to red indicate that the 100 year return level for MaxRunSum3 will be lower (drier) in the future than in the common period. And, any blue colours indicate that the 100 year return level will be higher (wetter) in the future.

Because of differences in the areas affected by undefined GEV mean and variance between the models, it is difficult/impossible to create meaningful results for an average model and estimate confidence limits. A common feature is that one in 100 year events will be less wet in Turkey, Greece, much of Italy, and southern Spain under the A2a scenario. Although all models indicate increased extreme rainfall over northern Spain under A2a, the amount varies by about 100 mm

between them. The main influence of the B2a scenario is to moderate the A2a increases in 100-year rainfall. However, the B2a has little effect on areas showing less rainfall under the A2a scenario.

**Differences (mm of rainfall) in 100 year return levels of MaxRunSum3 between the common period and the A2a and B2a scenarios**

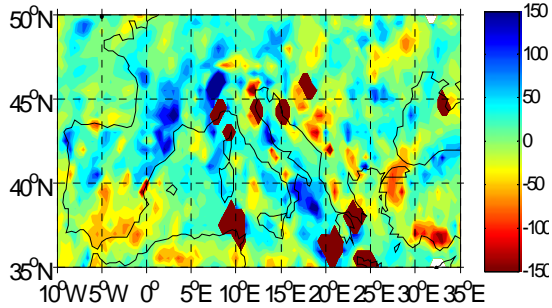


Figure 10a HadRM3P A2a

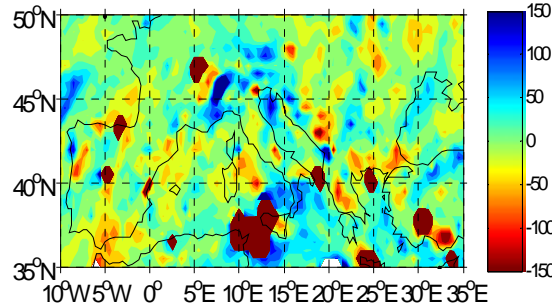


Figure 10b HadRM3P B2a

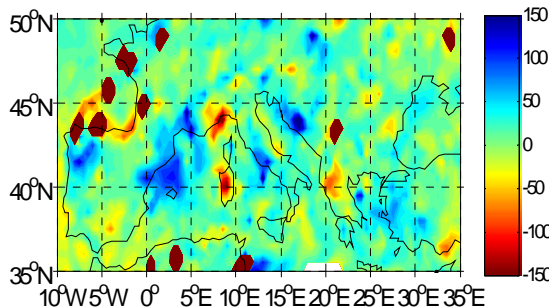


Figure 11a SMHI-HC A2a

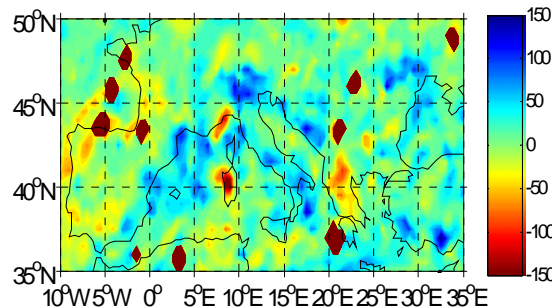


Figure 11b SMHI-HC B2a

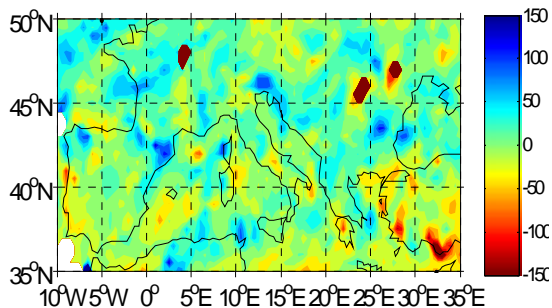


Figure 12a SMHI-MPI A2a

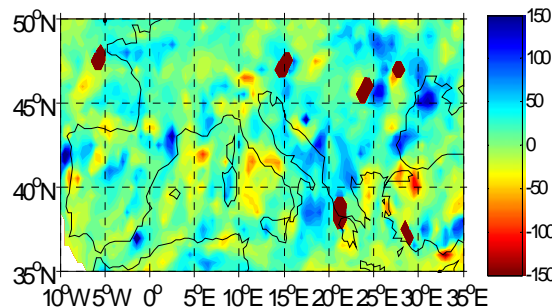


Figure 12b SMHI-MPI B2a

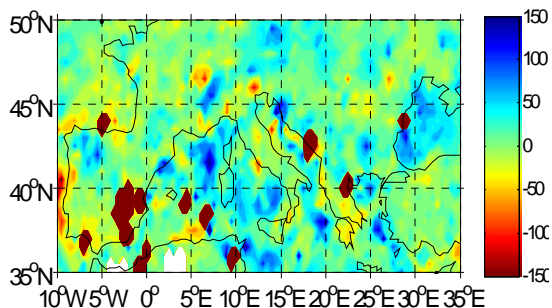


Figure 13a DMI A2a

## 5.2 MaxWetSpell

The differences in 100-year return levels of maximum length of wet spell (Figures 14a to 17a) show that under the A2a scenario, Mediterranean countries can generally expect a reduction by up to 14 days. The only exception is the SMHI model under HC forcing (Figure 15a), which offers an increase of about 20 days over northern Portugal. It is likely that this is an artifact of spurious sensitivity in the model physics. The B2a scenario (Figures 14b to 16b) also indicates shortening of the one in 100-year event, but the shortening is reduced by about 5 days compared with the A2a scenario.

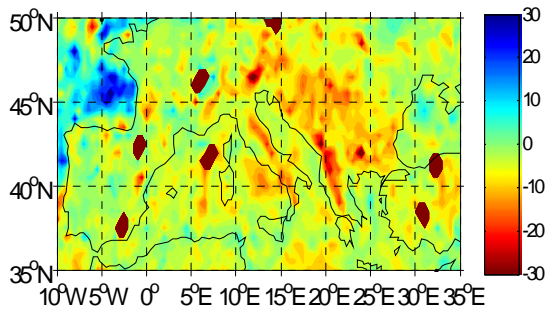


Figure 14a HadRM3P A2a

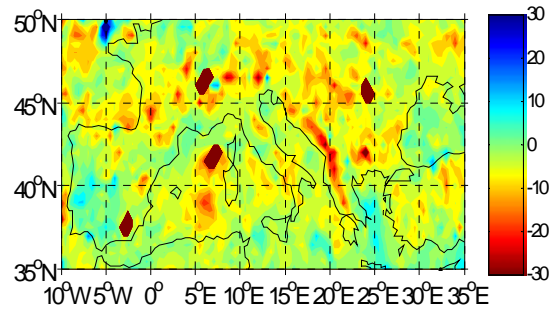


Figure 14b HadRM3P B2a

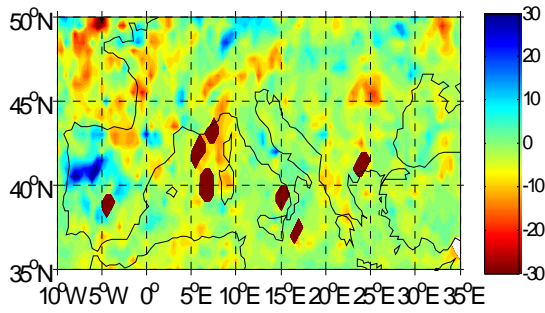


Figure 15a SMHI-HC A2a

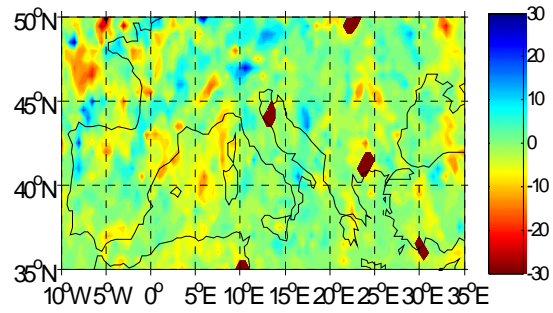


Figure 15b SMHI-HC B2a

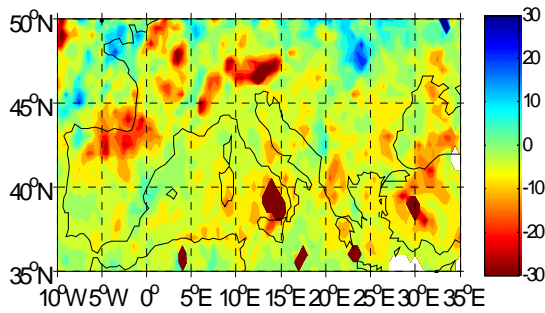


Figure 16a SMHI-MPI A2a

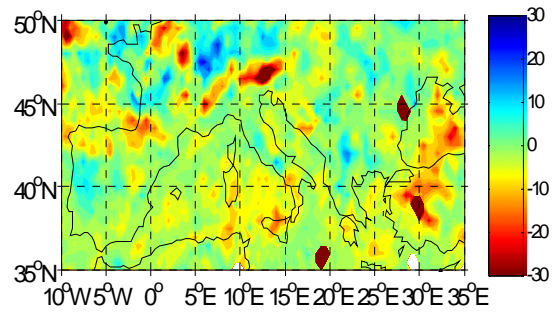


Figure 16b SMHI-MPI B2a

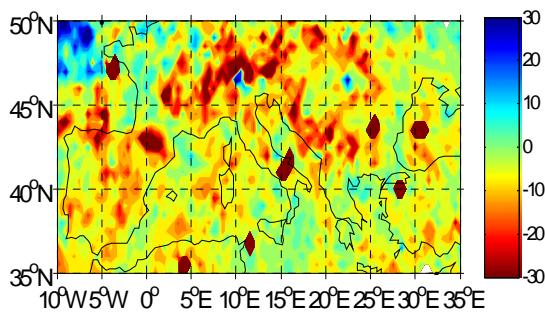


Figure 17a DMI A2a

### 5.3 MaxDrySpell

The differences for the 100-year maximum length of dry spell (Figures 18a to 21a) reveal a methodological inconsistency. In many places, the MaxDrySpell may be, for example, 150 days during the common period. Yet the differencing gives values as high as 300 days – implying a year with 450 days. The problem is that the return level routine does not know that a model year only has 360 days. Where the maximum dry spell difference becomes red, therefore, it is safe to assume there are no wet days in the year. Note that in these figures, the areas with invalid GEV parameters are now dark blue because the colour scaling has been reversed. The white areas in Figures 19a to 21a also represent areas with a poor fit to the GEV model.

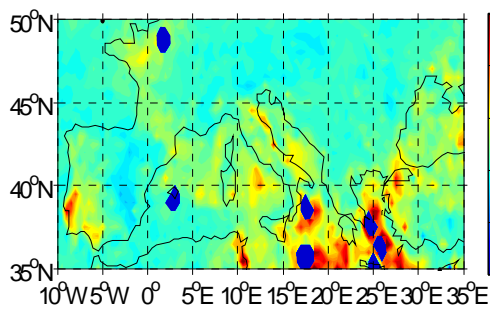


Figure 18a HadRM3P A2a

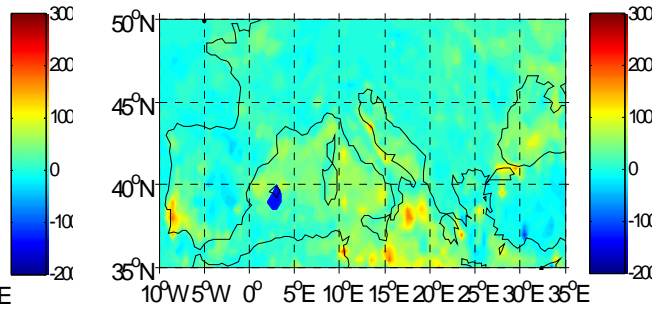


Figure 18b HadRM3P B2a

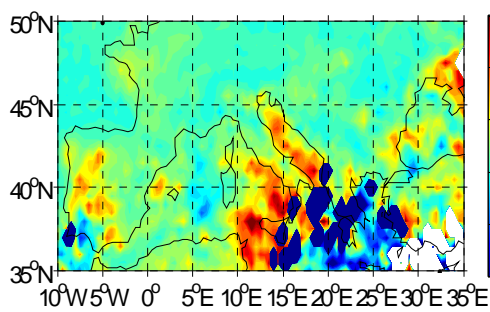


Figure 19a SMHI-HC A2a

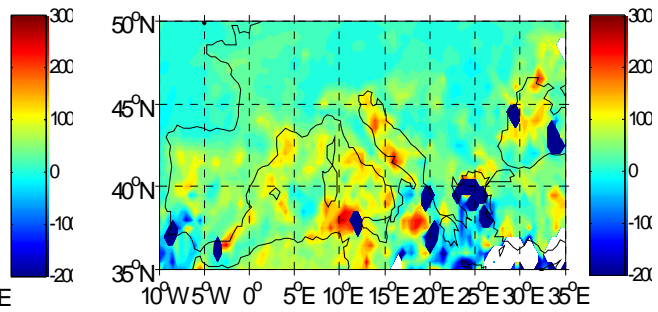


Figure 19b SMHI-HC B2a

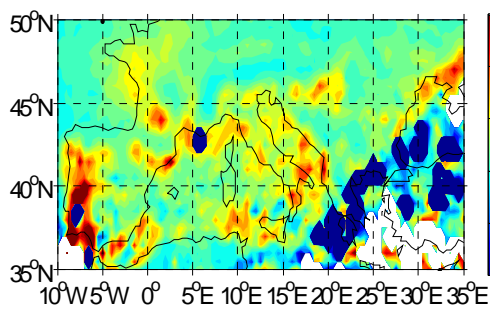


Figure 20a SMHI-MPI A2a

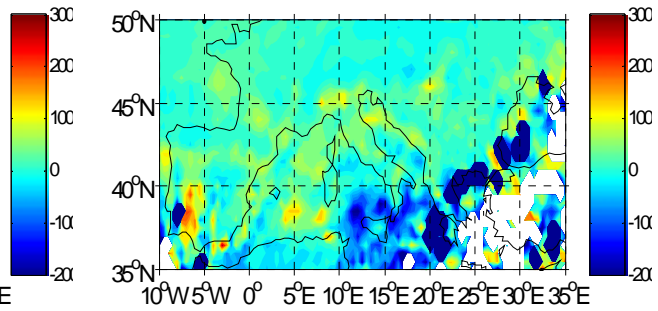


Figure 20b SMHI-MPI B2a

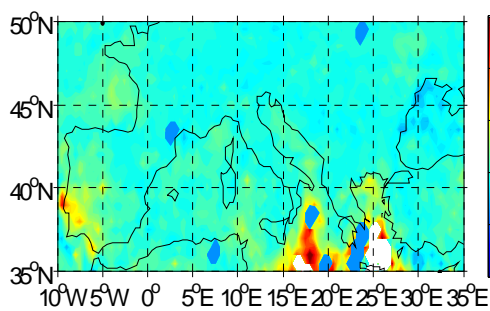


Figure 21a DMI A2a

The areas with longer drought in the 100-year return levels (Spain and Italy) vary by about 100 days between models for the A2a scenario (Figures 18a to 21a). The extension of the drought is much reduced under the B2a scenario (Figures 18b to 20b). The only region showing a future reduction in the length of the 100-year maximum dry spell is over the sea to the southeast of Italy for the SMHI models (Figures 19a and 20a). The same area has longer MaxDrySpell for the HadRM3P and DMI models (Figures 18a and 21a, respectively). Under the B2a scenario, the 100-year return level differences for MaxDrySpell are shortened by about 100 days over much of the western and central Mediterranean, with larger changes seen in the SMHI model.

## 6 Summary and Conclusions

Seven annual indices of rainfall extremes have been used to examine changes in rainfall extremes over the Mediterranean under climatic change. The indices are derived from the output of four Regional Climate Models (RCMs) and are sufficiently similar to allow averaging of the results to form a “model of models”. This has the advantage that uncertainty can be estimated based on the total variance across the models rather than simply the variability within a single model. Uncertainty is assessed by computing confidence limits using bootstrapping.

For each index, the mean difference between the A2a and B2a scenarios (2070-2100) and data for the common period (1960-1990) is calculated over all model years, together with the 95% confidence limit in the mean difference. An important finding is that changes in forcing due to different forcing models cause changes in future precipitation of the same order as changes due to the difference in forcing between the A2a and B2a emissions scenarios.

Predicted changes in precipitation indices between the periods 1960-1990 and 2070-2100, under the A2a emissions scenario, indicate considerable drying in the future over much of the Mediterranean. The main features are reduced intensity rainfall, earlier start of drought, and longer drought. The regions most affected are the southern Iberian peninsula, the Alps, the eastern Adriatic seaboard, and southern Greece. Although the B2a scenario provides considerable reduction in impacts, being associated with increased rainfall in some areas, the overall pattern is still one of a drier Mediterranean.

Generally, the most extreme changes have the highest uncertainty (up to about  $\pm 60\%$ ) but, on average, uncertainty at the 95% level is about  $\pm 20\%$ .

The analysis can be extended beyond the range of the available data by using the properties of the Generalized Extreme Value (GEV) distribution to assess return levels of annual maxima for particular return periods. Changes in return levels due to climate change are of particular interest. The analysis indicates that, for the A2a scenario, the 100-year return level for maximum total rainfall over three days will increase by about 100 mm over much of the Mediterranean. Under the B2a scenario, the increase is halved. The 100-year return level for maximum length of wet spell is reduced by up to 20 days under the A2a scenario but by less than 10 days under the B2a scenario. Under the A2a scenario, the 100-year return level for the maximum longest dry spell is increased everywhere and, in places, persists throughout the year. The B2a scenario reduces this maximum to about 250 days. Because of an inconsistency in the methodology, it is better to consider the maximum length of dry spell in terms of the change in return period of a given level rather than using the 100-year return period.

This analysis describes the effects of climate change on Mediterranean precipitation in 2070-2100. There is sufficient agreement between the spatial patterns of the models used to have reasonable confidence in the results. The main concern is that a change in forcing model causes a change in precipitation between 1960-1990 and 2070-2100 of the same magnitude as the change in precipitation due to changing forcing from the A2a to B2a scenario. Testing with more models using different forcing is essential before drawing definite conclusions about the influence of this factor on total inter-model variability.

## 7 Appendix

This Appendix presents detailed comparisons between all models for all extreme indices. It is included to confirm that, by and large, there are no serious inconsistencies in the model predictions. All the maps show the differences between the 1960-1990 period mean extremes and the 2070-2100 period mean extremes.

### 7.1 *nGT10 differences*

Figures 22a and 22b indicate that HadRM3P predicts little change in the number of days with rainfall higher than 10 mm. Mountainous areas, on the other hand, can expect a reduction of 10 to 15 days with rainfall over this threshold. The B2a scenario is slightly drier than the A2a scenario. The SMHI model with Hadley Centre Forcing (Figures 22c and 22d) gives very similar results to HadRM3P, but the B2a scenario shows considerably less drying than the A2a. With MPI forcing (Figures 22e and 22f), the SMHI model shows a much greater reduction in the number of wet days. Interestingly, the effect of the change in forcing is about the same as the difference between the scenarios (compare Figures 22c and 22f with each other and with Figure 22e). Figure 22g shows that the DMI model has a much weaker difference pattern for nGT10 than the other models, with no change associated with high ground.

### 7.2 *nGT20 differences*

HadRM3P again picks out mountainous regions as having future reductions in rainfall (Figures 23a and 23b). Unusually, the B2a scenario shows a slightly greater reduction than the A2a scenario. The SMHI model with HC forcing (Figures 23c and 23d) presents little evidence of change with this higher rainfall threshold. SMHI with MPI forcing, on the other hand, shows a considerable reduction in rainfall over high ground with the A2a scenario (Figure 23e). This is much reduced under the B2a scenario (Figure 23f). The DMI model shows little evidence of change in the frequency of heavy rainfall events (Figure 23g).

### 7.3 *MaxDrySpell differences*

Figures 24a to 24f show that a common feature of future changes in the length of the maximum dry period is a tendency for longer drought in southern Portugal and the eastern Mediterranean (HadRM3P and SMHI model with HC forcing, Figures 24a and 24c) and for western France and the central Mediterranean with the SMHI model and MPI forcing (Figure 24e). The increased length of drought in southern Portugal is much more pronounced with MPI forcing (Figure 24e). In all cases, the increase in drought is much reduced under the B2a scenario (Figures 24b, 24c, and 24f). Again, the DMI model has a much weaker difference pattern than the other models (Figure 24g).

We now consider whether future changes in maximum length of dry spell occur earlier or later than in the common period.

### 7.4 *StartDrought differences*

The colouring convention for the StartDrought plots (Figures 25a to 25g) requires some explanation. Negative values indicate that the maximum dry spell occurs earlier in the future than in the present day. Since this could be associated with a longer dry spell we colour negative values red/yellow to indicate dryer conditions.

The pattern for HarRM3P A2a scenario (Figure 25a) divides the map diagonally from the southwest to the northeast. The southeastern half has the maximum dry spell starting earlier in the future, and the northwestern half starts later. The B2a scenario has the same pattern but the displacement of the drought is much less (Figure 25b). The patterns formed by the SMHI and DMI models (Figures 25c to 25g) divide the domain north/south with later onset of drought in the north and earlier in the south.

**nGT10**

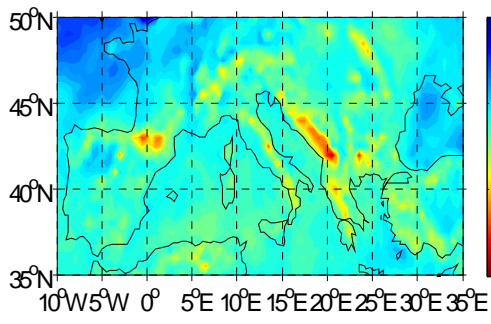


Figure 22a  
HadRM3P A2a - nGT10

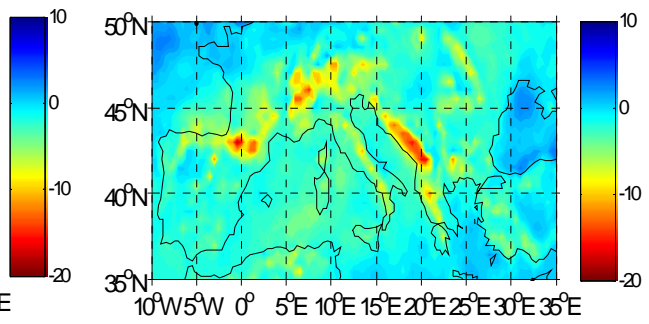


Figure 22b  
HadRM3P B2a - nGT10

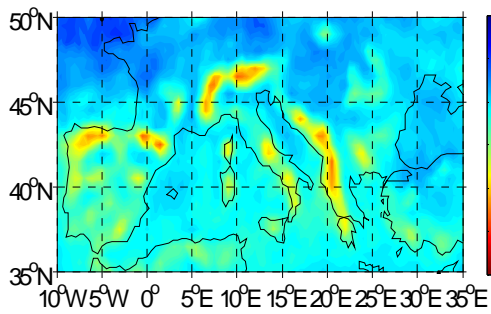


Figure 22c  
SMHI HC forcing A2a - nGT10

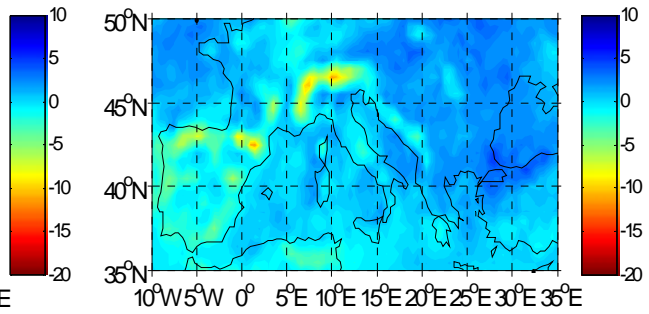


Figure 22d  
SMHI HC forcing B2a - nGT10

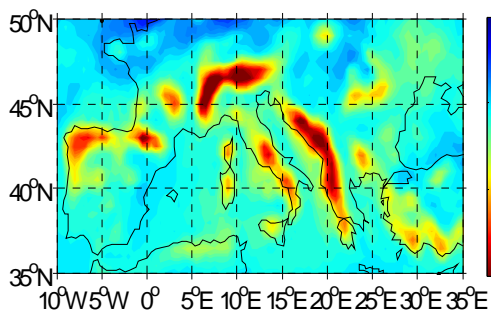


Figure 22e  
SMHI MPI forcing A2a - nGT10

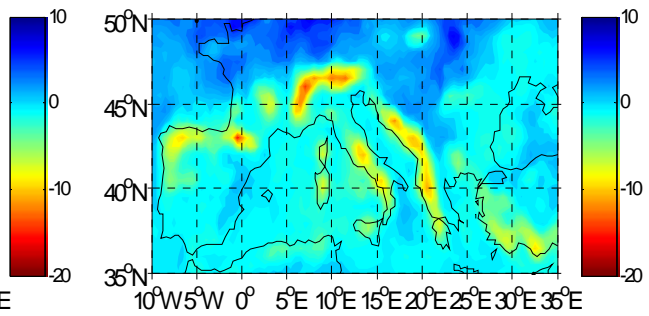


Figure 22f  
SMHI MPI forcing B2a - nGT10

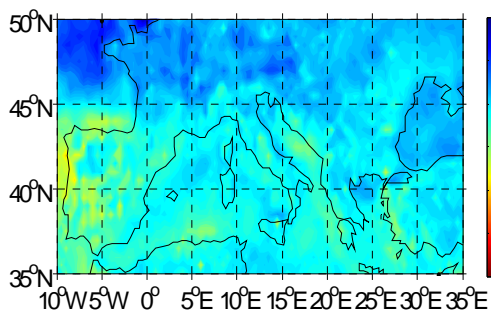


Figure 22g  
DMI HC forcing A2a - nGT10

**nGT20**

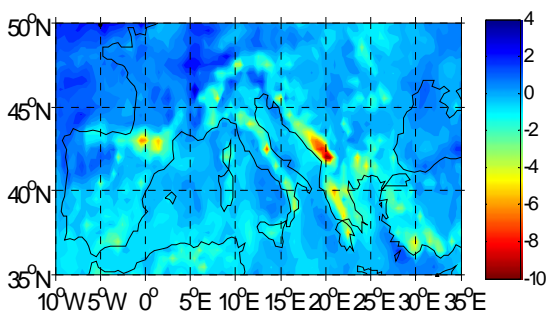


Figure 23a

HadRM3P A2a - nGT20

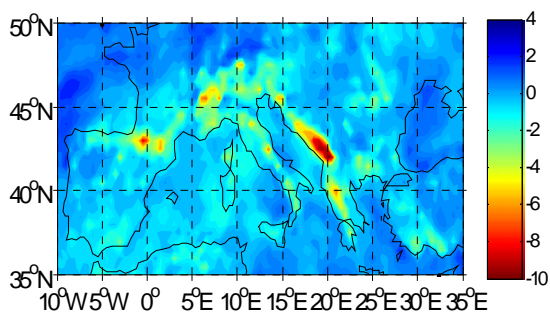


Figure 23b

HadRM3P B2a - nGT20

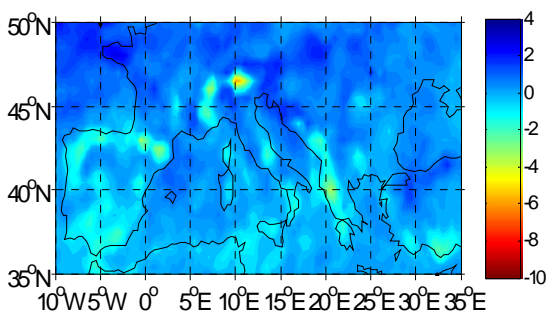


Figure 23c

SMHI HC forcing A2a - nGT20

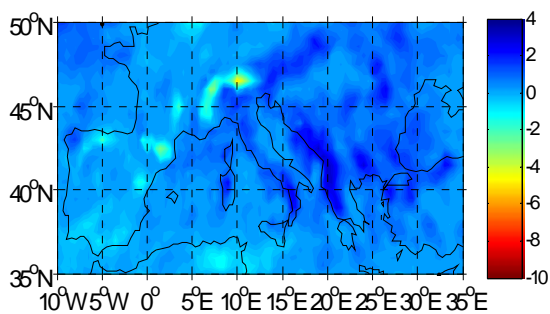


Figure 23d

SMHI HC forcing B2a - nGT20

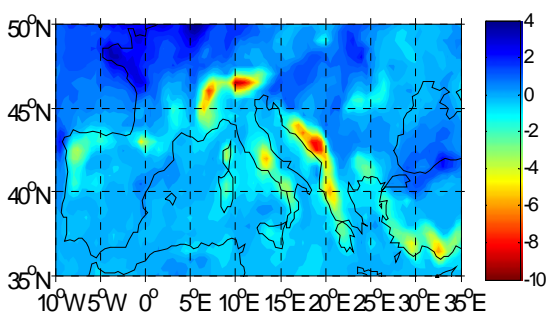


Figure 23e

SMHI MPI forcing A2a - nGT20

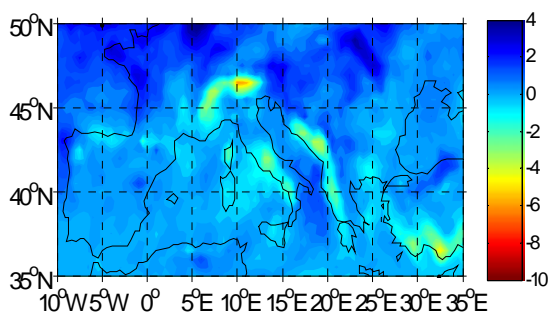


Figure 23f

SMHI MPI forcing B2a - nGT20

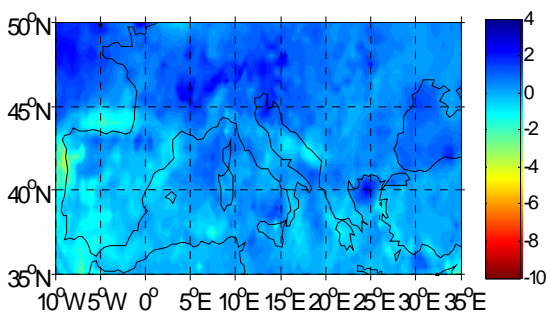


Figure 23g

DMI HC forcing A2a - nGT20

### MaxDrySpell

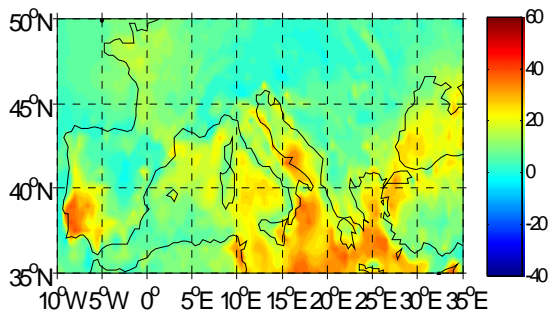


Figure 24a

HadRM3P A2a - MaxDrySpell

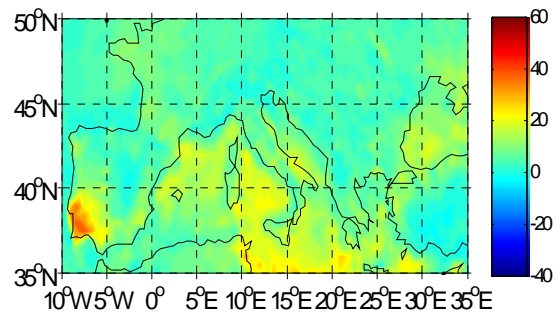


Figure 24b

HadRM3P B2a - MaxDrySpell

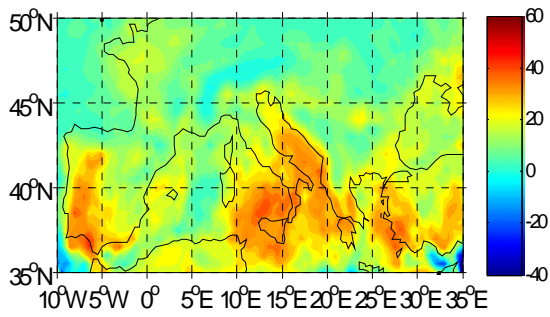


Figure 24c

SMHI HC forcing A2a - MaxDrySpell

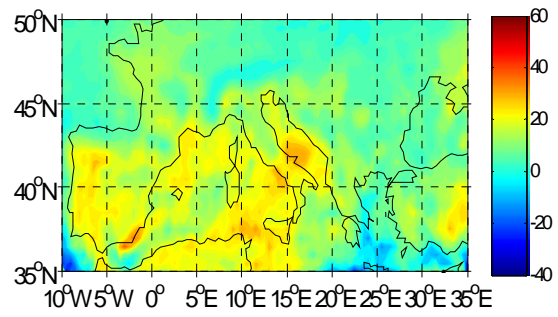


Figure 24d

SMHI HC forcing B2a - MaxDrySpell

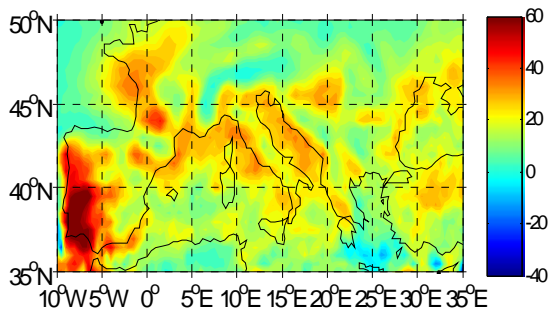


Figure 24e

SMHI MPI forcing A2a - MaxDrySpell

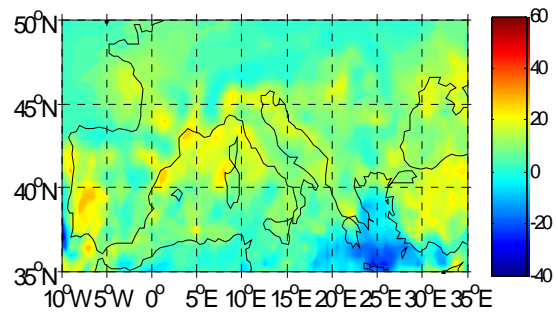


Figure 24f

SMHI MPI forcing B2a - MaxDrySpell

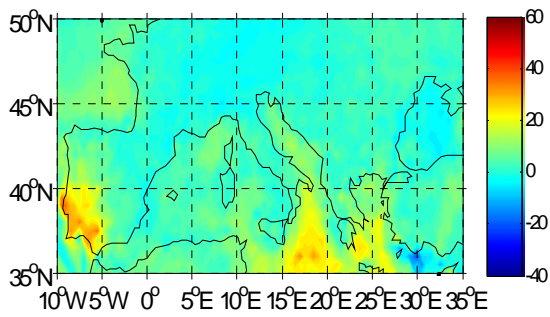


Figure 24g

DMI HC forcing A2a - MaxDrySpell

### StartDrought

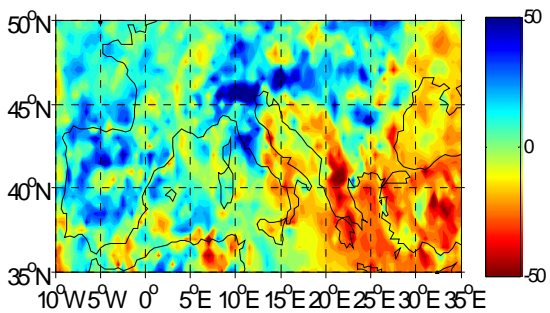


Figure 25a

HadRM3P A2a - StartDrought

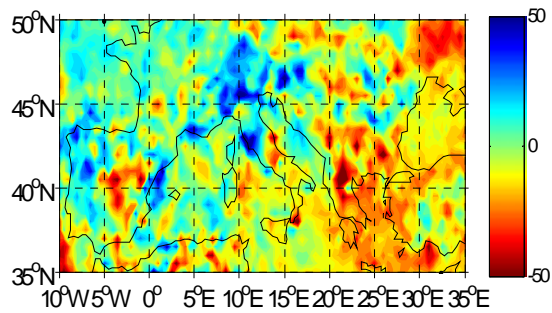


Figure 25b

HadRM3P B2a - StartDrought

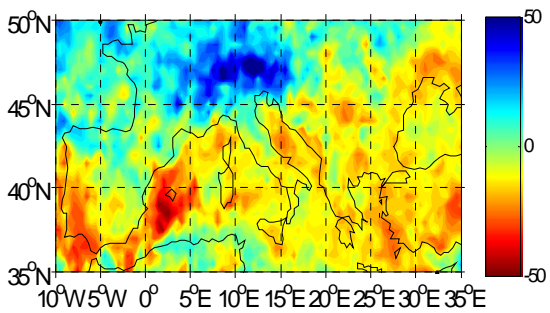


Figure 25c

SMHI HC forcing A2a - StartDrought

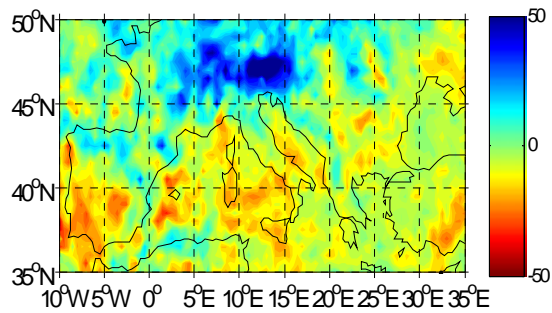


Figure 25d

SMHI HC forcing B2a - StartDrought

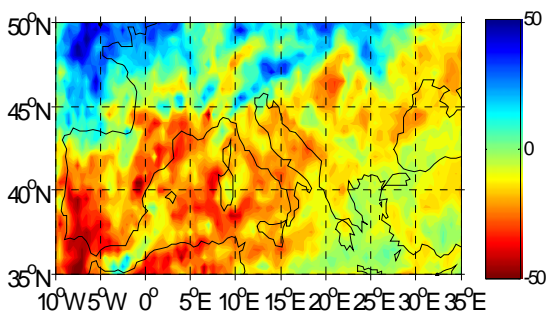


Figure 25e

SMHI MPI forcing A2a - StartDrought

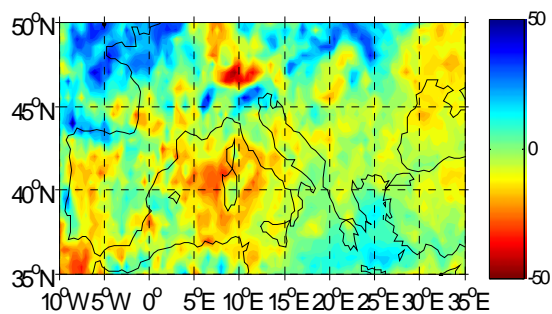


Figure 25f

SMHI MPI forcing B2a - StartDrought

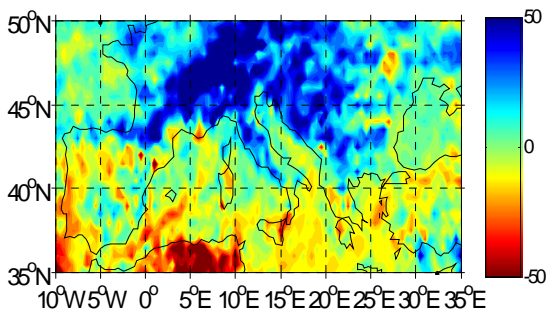


Figure 25g

DMI HC forcing A2a - StartDrought

## **7.5 EndDrought differences**

The plots of end of maximum dry period (Figures 26a to 26g) reverse the colour scheme used for start of drought. Positive values indicate a later future end of drought, implying possible drier conditions, and are coloured red/yellow.

The HadRM3P model (Figures 26a and 26b) shows a later future end of drought for much of the domain in both scenarios. The SMHI model (Figures 26c to 26f) has much later end of drought over France and Switzerland with HC forcing (Figures 26c and 26d), and over the northwest of the domain with MPI forcing (Figures 26e and 26f). The DMI model (Figure 26g) has much later future end of drought over the northern part of the domain.

## **7.6 MaxWetSpell differences**

The patterns of maximum wet spell differences for HadRM3P and SMHI with HC forcing show little change in future (Figures 27a to 27d), with the biggest changes being a reduction of the order of four or five days mainly over high ground. The magnitude of this change doubles with the SMHI model and MPI forcing under the A2a scenario (Figure 27e), with the pattern weakened under the B2a scenario (Figure 27f). The DMI model also shows a reduction of the order of 10 days in the maximum wet spell (Figure 27g), with the biggest changes over northern Spain, the Alps, the eastern Adriatic, and northern Greece.

## **7.7 MaxRunSum3 differences**

The maximum running total rainfall over three days is predicted to be reduced over southern Spain, north Africa, the eastern Adriatic, Greece, and Turkey, according to the HadRM3P A2a scenario (Figure 28a). Rainfall is shown to increase by up to 40 mm over northern Spain, southern France, and Italy. Under the B2a scenario, the rainfall increases over northern Spain and southern France are largely removed (Figure 28b), but rainfall increases by up to 60 mm over Libya. The SMHI model with HC forcing has reduced future rainfall over southern Spain but shows increases over much of the northern Mediterranean for the A2a scenario (Figure 28c). Under the B2a scenario (Figure 28d), the pattern is repeated but with reduced intensity. The pattern for MPI forcing of the SMHI model (Figures 28e and 28f) is similar to that for HC forcing but with a smaller increase in rainfall. The DMI model (Figure 28g) has a difference pattern similar to that for the SMHI model with HC forcing, but with rainfall increasing to 30 mm.

### EndDrought

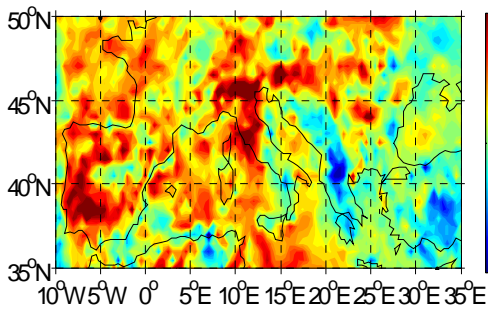


Figure 26a

HadRM3P A2a - EndDrought

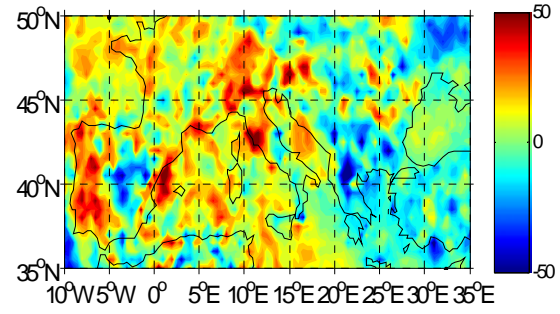


Figure 26b

HadRM3P B2a - EndDrought

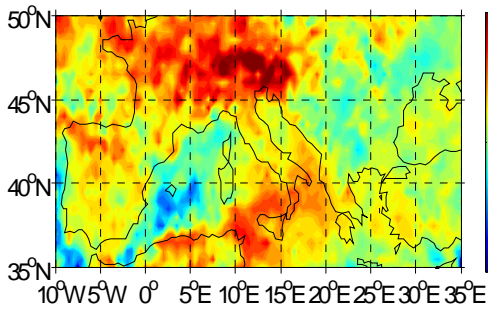


Figure 26c

SMHI HC forcing A2a - EndDrought

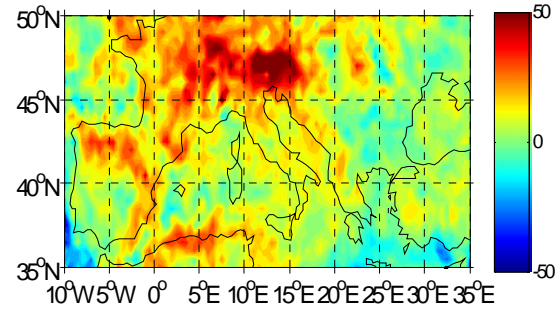


Figure 26d

SMHI HC forcing B2a - EndDrought

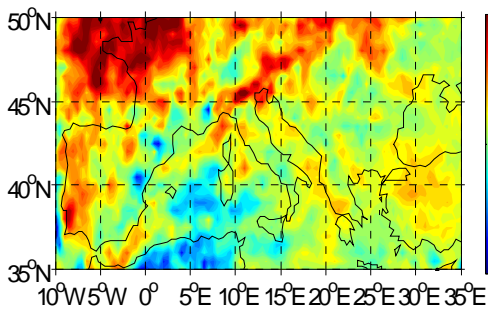


Figure 26e

SMHI MPI forcing A2a - EndDrought

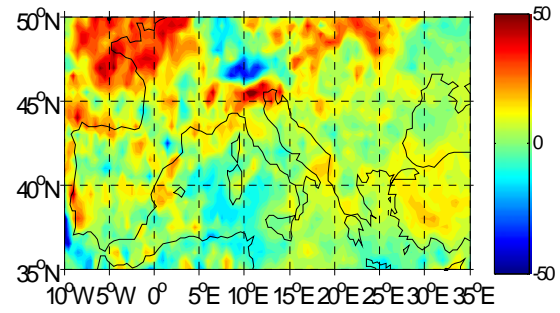


Figure 26f

SMHI MPI forcing B2a - EndDrought

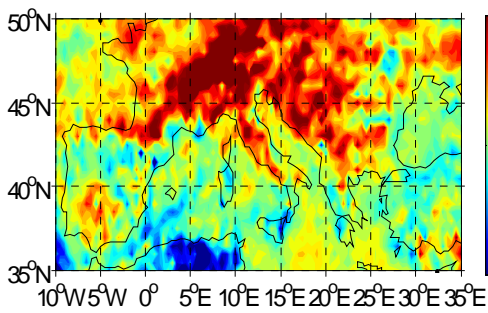


Figure 26g

DMI HC forcing A2a - EndDrought

### MaxWetSpell

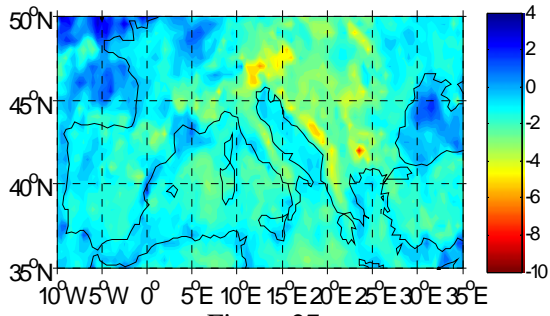


Figure 27a

HadRM3P A2a - MaxWetSpell

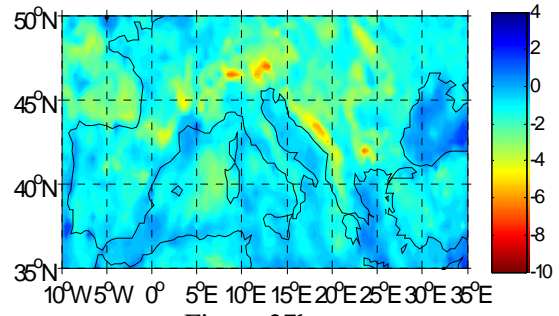


Figure 27b

HadRM3P B2a - MaxWetSpell

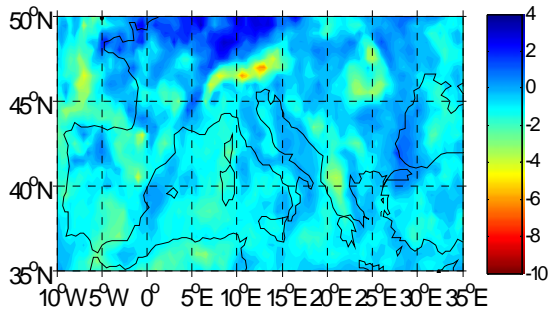


Figure 27c

SMHI HC forcing A2a - MaxWetSpell

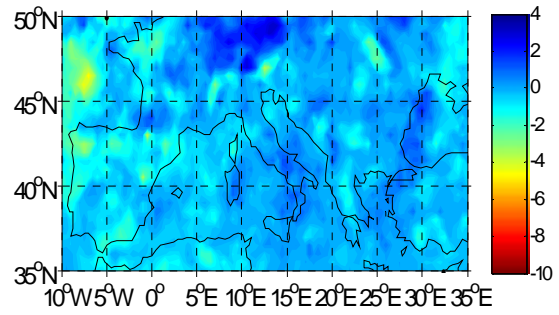


Figure 27d

SMHI HC forcing B2a - MaxWetSpell

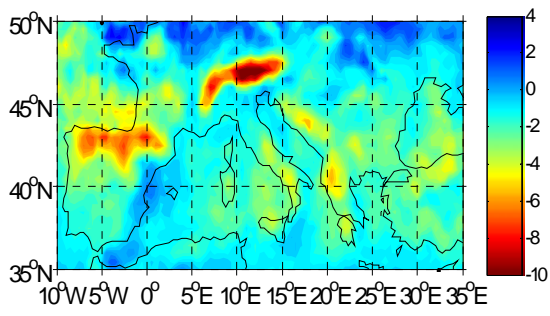


Figure 27e

SMHI MPI forcing A2a - MaxWetSpell

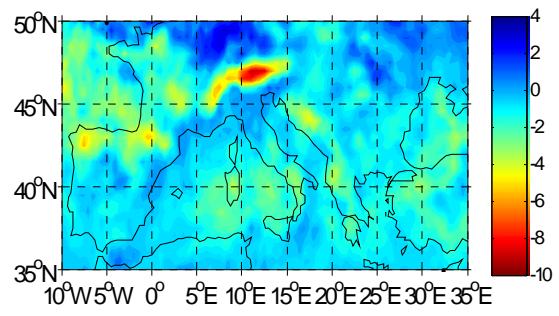


Figure 27f

SMHI MPI forcing B2a - MaxWetSpell

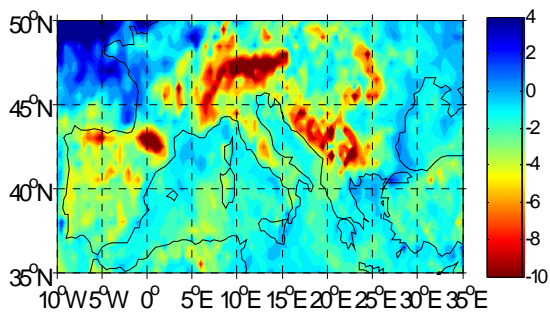


Figure 27g

DMI HC forcing A2a - MaxWetSpell

### MaxRunSum3

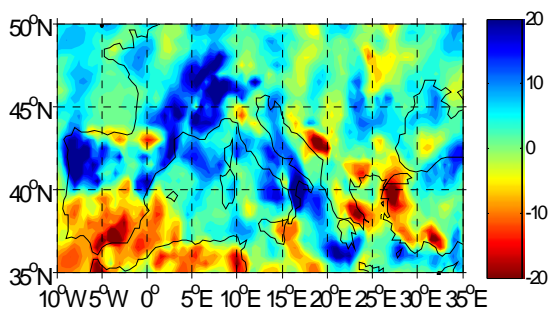


Figure 28a

HadRM3P A2a - MaxRunSum3

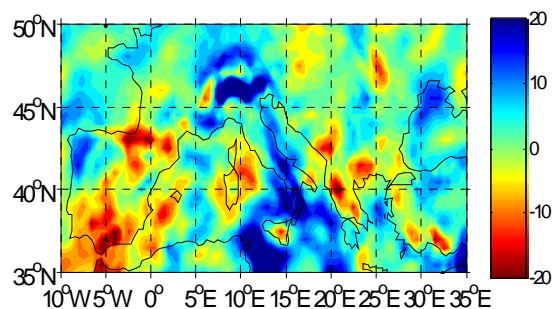


Figure 28b

HadRM3P B2a - MaxRunSum3

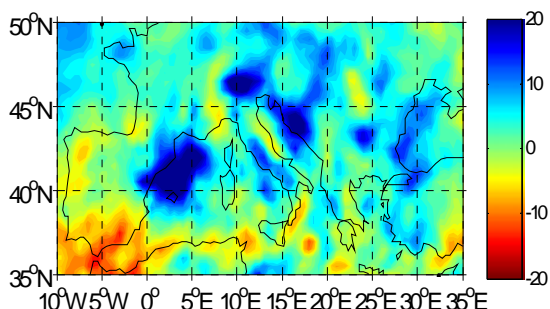


Figure 28c

SMHI HC forcing A2a - MaxRunSum3

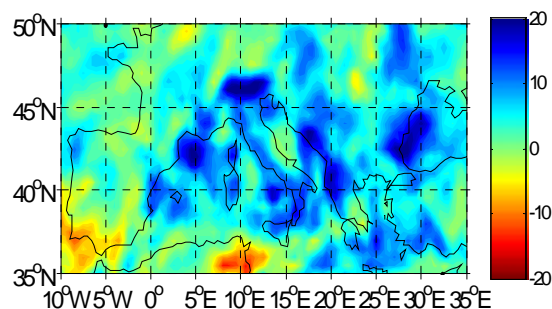


Figure 28d

SMHI HC forcing B2a - MaxRunSum3

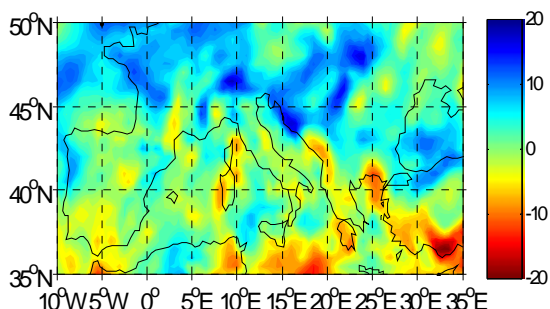


Figure 28e

SMHI MPI forcing A2a - MaxRunSum3

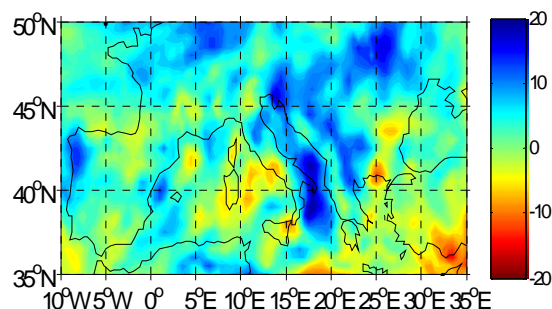


Figure 28f

SMHI MPI forcing B2a - MaxRunSum3

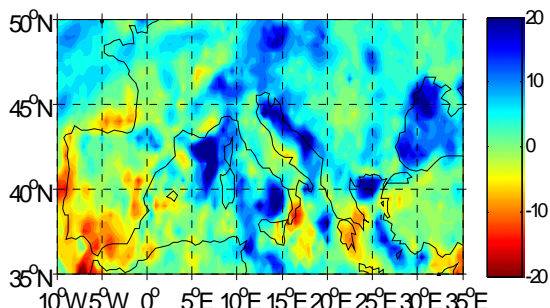


Figure 28g

DMI HC forcing A2a - MaxRunSum3

## References

- Coles, S. (2001): *An Introduction to Statistical Modeling of Extreme Values*. Springer-Verlag UK; ISBN: 1852334592, 222 pp.
- Davison, A.C. & D.V. Hinkley (1997): *Bootstrap Methods and Their Applications*. Cambridge Series in Statistical & Probabilistic Mathematics, Cambridge University Press; ISBN: 0521574714, 592 pp.